Journal Pre-proof

A Double-Sigmoid Approach for High-Throughput Phenotyping of Winter Wheat Growth Dynamics

Shannon Baker , Lei Zhao , Jose Landivar Scott , Jackie Rudd , Amir MH Ibrahim , Juan Landivar , Jinha Jung , Shuyu Liu , Kevin Nowka , Mahendra Bhandari

PII: S2772-3755(26)00172-3
DOI: https://doi.org/10.1016/j.atech.2026.101948
Reference: ATECH 101948

To appear in: *Smart Agricultural Technology*

Received date: 13 October 2025
Revised date: 3 March 2026
Accepted date: 4 March 2026

Please cite this article as: Shannon Baker , Lei Zhao , Jose Landivar Scott , Jackie Rudd , Amir MH Ibrahim , Juan Landivar , Jinha Jung , Shuyu Liu , Kevin Nowka , Mahendra Bhandari , A Double-Sigmoid Approach for High-Throughput Phenotyping of Winter Wheat Growth Dynamics, *Smart Agricultural Technology* (2026), doi: https://doi.org/10.1016/j.atech.2026.101948

A Double-Sigmoid Approach for High-Throughput Phenotyping of Winter Wheat Growth Dynamics

Shannon Baker[1], Lei Zhao[2], Jose Landivar Scott[2], Jackie Rudd[1], Amir MH Ibrahim[3], Juan Landivar[2], Jinha Jung[4], Shuyu Liu[3], Kevin Nowka[5], and Mahendra Bhandari[2*]

[1]Texas A&M AgriLife Research, 6500 W Amarillo Blvd. Amarillo, TX, 79106 United States.

[2]Texas A&M AgriLife Research, 10345 TX-44 Corpus Christi, TX, 78406 United States.

[3]Texas A&M AgriLife Research, 600 John Kimbrough Blvd College Station, TX 77843 United States.

[4]Lyles School of Civil and Construction Engineering, Purdue University, 550 Stadium Mall Drive West Lafayette, IN 47907-2051 United States.

[5]Texas A&M University, 400 Bizzell St, College Station, TX 77843 United States.

* Corresponding author

Abstract

Multi-temporal data from unoccupied aerial systems (UAS) offer insights into growth parameters for winter wheat breeding decisions. Weekly UAS data were collected during the 2019 and 2020 growing seasons from dryland and irrigated nurseries at Bushland, Texas, within the Texas A&M Uniform Variety Trials. Canopy cover (CC) was extracted from orthomosaic images and modeled using a double-sigmoid function with a second-order derivative that captured genotypic variation in canopy growth and senescence with high coefficients of determination ($R^2 > 0.99$) and low root mean square error (RMSE) values ranging from 1.73 to 4.06. Analysis of variance (ANOVA) revealed highly significant genotypic effects ($p<0.001$) for yield, heading, and Green Leaf Area Duration (LAD) in all environments except 2020 dryland, where no significant differences among genotypes were detected. Extracted parameters showed positive correlations with agronomic traits, particularly under rainfed and stress-prone conditions. The end decrease stage (EDS) was correlated with grain yield ($r=0.56$ in 2019 dryland, and $r=0.53$ in 2020 irrigated, $p<0.001$), and the start decrease stage (SDS) was highly correlated with yield ($r=0.53$ in 2020 irrigated, $p<0.001$). The maximum decrease rate date (MDRD) was positively correlated with yield in 2019 dryland ($r=0.55$, $p<0.001$), while LAD had a correlation of $r=0.56$ in 2019 dryland and $r=0.58$ in 2020 irrigated ($p<0.001$). These findings demonstrate that double-sigmoid model provides a powerful, non-invasive framework for quantifying canopy development, senescence timing, and stress responses. By distinguishing genetics from environmental influences on canopy dynamics, this approach enhances selection accuracy and accelerates the development of stress-resilient winter wheat cultivars.

Key Words

High-throughput phenotyping, UAS, Winter Wheat, Double-sigmoid model, Canopy Cover, Growth Dynamics, Plant Breeding

1.0 Introduction

Winter wheat (*Triticum aestivum* L.) is a critical component of global agriculture and a major dual-purpose crop in Texas, where it is planted on 2.5 million hectares [1]. It supports vital livestock systems and contributes substantially to grain production for human consumption with an average grain yield of 2.9 T ha^{-1} [2]. The combined demand for forage, fodder, fiber, and grain makes the accelerated development of high-yielding, climate-resilient crop cultivars imperative. High-throughput phenotyping (HTP) technologies, particularly unoccupied aerial systems (UAS), are transforming this process by enabling rapid, precise, and non-destructive assessment of complex traits, thereby enhancing selection accuracy [3–5]. UAS imagery enables the construction of fine-grained growth curves by extracting plot-level traits from multi-temporal flights for multi-temporal analysis [6]. In winter wheat, dynamic traits like canopy cover (the percentage of ground covered by green vegetation; CC), heading, and senescence timing are critical for yield and stress adaptation, and UAS provides an objective alternative to low-throughput traditional measurements [7–10].

The developmental trajectory of winter wheat typically follows a sigmoid (S-shaped) growth pattern, characterized by distinct phases of establishment, rapid spring growth, a plateau around heading, and finally, senescence [11,12]. Consequently, mathematical growth models are essential for quantifying these dynamic traits across large breeding trials [13]. Sigmoidal models, such as the logistic function, are well-established for describing plant and canopy growth over time, as they accurately capture the slow-start, rapid-growth, and saturation phases [14,15]. By fitting these curves to multi-temporal UAS-derived phenotypic traits, plant breeders can extract biologically meaningful parameters, such as maximum growth rate (MGR) and the timing of the inflection point, to compare genotypic performance. Recent work has demonstrated the feasibility of applying these models at scale in breeding pipelines, using UAS-based data to quantify genetic differences in phenology [16–19].

A key application of this approach is estimating phenological events. For instance, Zhao et al. [20] compared nine sigmoid equations for modeling UAS-derived wheat growth and identified an optimal method to estimate heading dates from the fitted curves with a mean error of only 1-2 days. This demonstrates that canopy dynamics derived from UAS imagery can effectively represent key growth stages. However, a significant limitation of the single sigmoid function is its inability to model the full crop lifecycle. While it effectively captures the rapid expansion and stabilization of CC during vegetative growth, it fails to represent the subsequent decline in CC that occurs during senescence, when the greenness signal decreases rather than following a continued sigmoid trajectory. Valuable information about the senescence rate and canopy duration (DUR; defined as the number of days between the start and end of canopy saturation) which dictate the grain-filling period and therefore strongly influence final yield are omitted using a single curve.

To address this gap, this study proposes a double sigmoid model to offer a more comprehensive framework. The double sigmoid model is specifically designed to capture both the increase and decrease within one continuous curve, essentially joining an ascending curve for canopy growth (green-up) and a descending curve for canopy decline (senescence) [21]. Double-logistic functions have been widely used in satellite remote sensing to characterize vegetation phenology from NDVI time series, enabling the extraction of transition dates, such as the start of the season, peak greenness, and end of the season in corn and wheat [22,23]. Compared to a single logistic model, the double sigmoid's capacity to define two inflection points, one during green-up and one during senescence, is particularly advantageous for modeling the complete growth cycle of crops like winter wheat.

Previous UAS-based phenotyping studies have successfully applied single sigmoid or logistic functions to model canopy development or estimate specific phenological events such as heading date. These approaches are effective for characterizing early- to mid-season canopy expansion; however, they inherently assume an increase followed by saturation and therefore cannot represent the decline in CC associated with senescence. As a result, critical late-season processes, including the timing and rate of canopy decline, DUR, and post-anthesis persistence of green tissue, are either omitted or inferred indirectly using ad hoc thresholds or single-date measurements. This limitation restricts the biological interpretability of single sigmoid models for traits closely linked to grain filling and stress tolerance in winter wheat.

In contrast, a double sigmoid framework explicitly models both canopy expansion and senescence within a single continuous function, enabling direct quantification of growth and decline phases and their transition points. While double sigmoid models have been widely used with satellite-scale vegetation indices, their application to high-resolution, plot-level UAS CC data in breeding trials remains limited. By leveraging first and second derivatives of a fitted double sigmoid curve, this study extends prior work by extracting a comprehensive set of phenologically meaningful traits that describe the complete crop life cycle and are directly relevant to selection under variable water availability.

Despite its potential, the application of double sigmoid functions to model high-resolution UAS-derived canopy development in winter wheat breeding remains underexplored. This represents a critical opportunity to improve the precision of HTP pipelines by characterizing the entire seasonal trajectory of canopy development. Therefore, this study aimed to characterize winter wheat CC growth with a double sigmoid curve function, exploring whether derivatives of the curve can be used to indirectly estimate multiple phenological changes that are important to wheat breeders.

2.0 Materials and Methods

2.1 Study Area

Winter wheat advanced yield trials (Texas Uniform Variety a.k.a. UVT trial) were planted in October 2018 and 2019, in dryland and sprinkler-irrigated nurseries on the Texas A&M AgriLife Research Experiment Station at Bushland, TX (35°11′ N, 102°06′ W, elevation 1170 m; Table 1). The trial comprised regionally adapted elite cultivars and was laid out in a Randomized Complete Block Design with three replications. The dryland (rainfed) trial had 28 entries in 2019 and 34 entries in 2020, while the irrigated trial had 34 entries in 2019 and 36 entries in 2020. Plots were 3.1 m × 1.5 m in size under irrigation and 4.5 m × 1.5 m under dryland conditions, with seven rows on 0.18 m spacing. Agronomic practices were implemented following regional guidelines; nutrients were managed for soil test-recommended yield goals, and weeds were controlled with herbicides as needed. The higher nitrogen rate applied in 2020 reflects soil test recommendations following the high precipitation 2019 season, leached residual soil nitrogen below the soil sampling depth. Nine semi-permanent 0.3 m × 0.3 m ground control points (GCPs) painted in a black and white checkerboard pattern were placed across the field after planting, and precise coordinates of the GCPs were surveyed using Trimble R8s Global Positioning System (GPS; Trimble Inc., Sunnyvale, CA, USA) receiver with real-time kinematic (RTK) corrections obtained via Texas Department of Transportation (TXDOT)'s Networked Transport of Radio Technical Commission for Maritime Service via Internet Protocol (NTRIP) network.

Table 1. Agronomic information including planting and harvest date, nitrogen (kg ha^{-1}) and irrigation applied (mm) of 2019-2020 Bushland dryland and irrigated trials.

	Dryland		Irrigation			
Year	Planting Date	Harvest Date	Planting Date	Harvest Date	Nitrogen (kg ha^{-1})	Irrigation (mm)
2019	Oct 20, 2018	June 26, 2019	Nov 15, 2018	July 3, 2019	67.3	88
2020	Oct 15, 2019	June 19, 2020	Oct 22, 2019	June 22, 2020	112.1	157

2.2 UAS Data Collection

UAS-data collection occurred throughout the eight-month growing season each year using a DJI Phantom 4 Pro equipped with an RGB sensor to capture canopy imagery in both the Bushland dryland and irrigated nurseries. RGB imagery was selected to derive CC because it provides a low-cost, widely accessible data source that can be readily deployed in breeding programs. Although multispectral imagery was available, using RGB-derived CC demonstrates that the proposed time-series framework can capture biologically meaningful canopy dynamics using imagery with a low barrier to entry.

UAS flights were conducted at approximately weekly intervals throughout the growing season, with higher frequency during periods of rapid canopy change (spring green-up and senescence) and fewer changes during periods of canopy saturation. While observation density was not explicitly balanced by phenological stage, the temporal resolution provided sufficient coverage of both vegetative and reproductive phases to support robust curve fitting across all environment-years. Flights were performed at an altitude of 20 m with 85% image overlap, resulting in image resolutions of approximately 20 megapixels and a ground sampling distance (GSD) of 0.55 cm pixel^{-1}. UAS data collection configuration and image processing settings to generate geospatial data products and CC were as described in Bhandari *et al.* (2021) and Bhandari *et al.* (2023).

Table 2 lists the calendar date and days after planting (DAP) of UAS data collections at Bushland dryland and irrigated nurseries. Precipitation, maximum temperature, and minimum temperature are shown in Figure 1 [24,25]. In 2019, total precipitation during the winter wheat season exceeded 475 mm, with consistent rainfall from planting through May. This provided optimal planting moisture and sustained soil water, resulting in normal to above-average yields and minimal irrigation requirements. In contrast, 2020 accumulated only about 380 mm of precipitation, roughly 20% less than in 2019, with limited rainfall from February through May. The deficit led to drought stress during stem elongation and grain filling, necessitating approximately twice the irrigation applied in 2019. Spring 2020 was also notably warmer, with average maximum temperatures 3-5 °C higher than in 2019 and more frequent daytime highs above 30°C. Minimum temperatures were likewise higher in late spring 2020, while 2019 maintained cooler nights throughout April and May. A late season freeze on April 13, 2020, further compounded stress during reproductive growth.

Table 2. Summary of unoccupied aerial data collection calendar date and days after planting (DAP) at Bushland irrigated and dryland wheat breeding nurseries in 2019 and 2020 growing seasons.

Irrigated				Dryland			
2019-2020		2020-2021		2019-2020		2020-2021	
Date	DAP	Date	DAP	Date	DAP	Date	DAP
9-Nov	4	11-Nov	4	22-Oct	0	31-Oct	9
28-Nov	23	28-Nov	23	4-Nov	13	14-Nov	23
10-Dec	35	17-Dec	42	14-Nov	23	25-Nov	34
17-Jan	73	17-Jan	73	25-Nov	34	3-Dec	42
26-Feb	113	26-Feb	113	3-Dec	42	13-Dec	52
15-Mar	130	15-Mar	130	13-Dec	52	14-Jan	84
24-Mar	139	24-Mar	139	15-Jan	85	24-Jan	94
29-Mar	144	29-Mar	144	24-Jan	94	31-Jan	100
4-Apr	150	4-Apr	150	30-Jan	100	17-Feb	118
8-Apr	154	9-Apr	155	17-Feb	118	24-Feb	125
16-Apr	162	16-Apr	162	24-Feb	125	2-Mar	132
24-Apr	170	24-Apr	170	2-Mar	132	10-Mar	140
1-May	177	1-May	177	10-Mar	140	22-Mar	152

6-May	182	6-May	182	22-Mar	152	31-Mar	161
13-May	189	13-May	189	31-Mar	161	7-Apr	168
19-May	195	19-May	195	7-Apr	168	17-Apr	178
24-May	200	30-May	206	17-Apr	178	23-Apr	184
30-May	206	3-Jun	210	23-Apr	184	29-Apr	190
3-Jun	210	10-Jun	217	29-Apr	190	14-May	205
10-Jun	217	17-Jun	224	14-May	205	29-May	210
17-Jun	224	24-Jun	231	19-May	210	27-May	218
24-Jun	231	30-Jun	237	27-May	218	3-Jun	225
				3-Jun	225	8-Jun	230
				8-Jun	230		

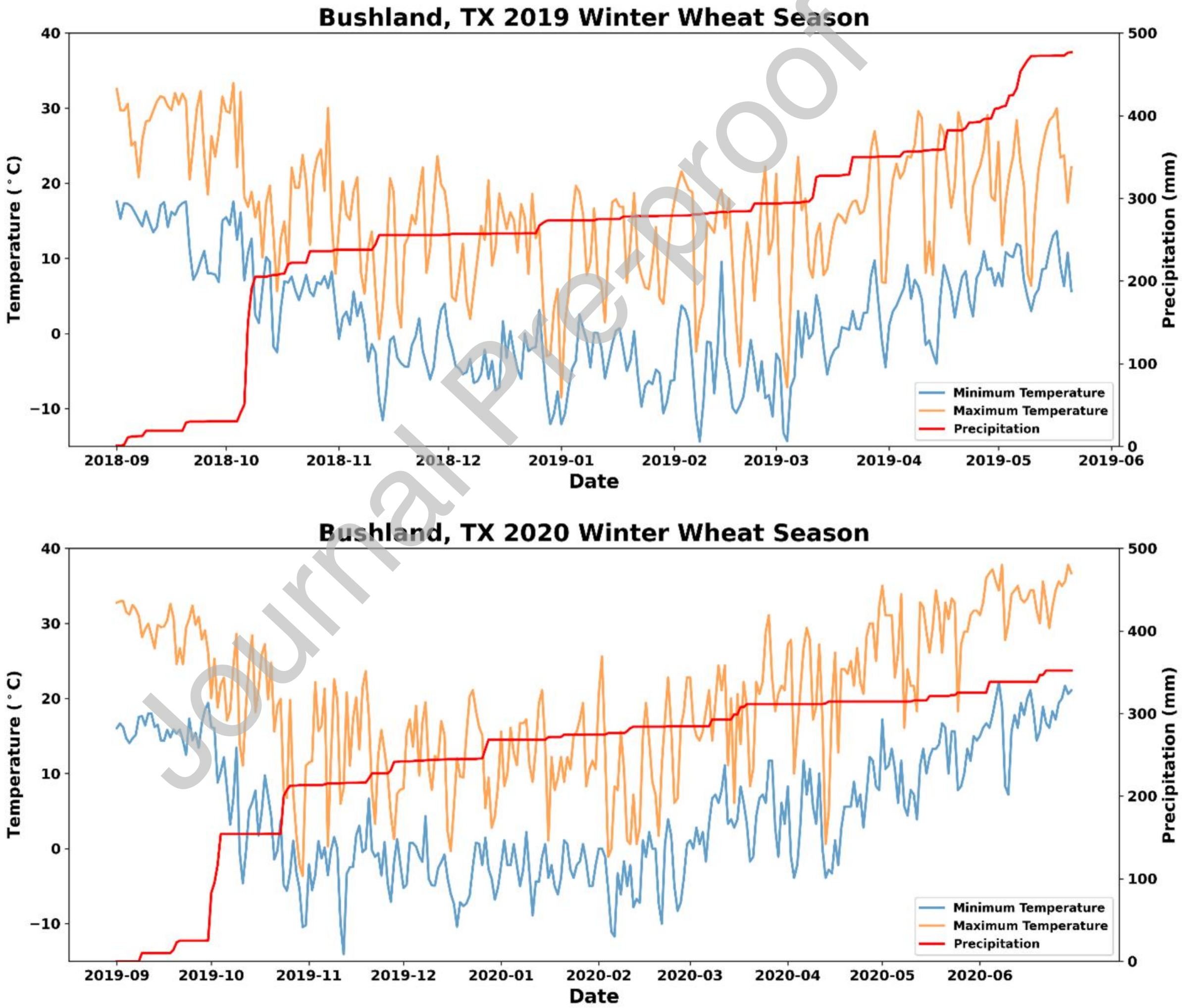

Figure 1. Daily minimum temperature (°C), maximum temperature (°C), and cumulative precipitation (mm) at USDA-ARS Bushland, TX during the 2019 and 2020 winter wheat growing season.

Manual phenotypic data were collected following standard breeding protocol. The heading date was recorded when 50% of the plot reached Feekes 10.3 stage [26] (DAP). Grain yield (T ha^{-1}) was obtained from Mirus HarvestMaster GrainGage software (Juniper Systems, Logan, UT) integrated into a Wintersteiger Classic small plot combine (Wintersteiger, Innkreis, Austria).

2.3 UAS Data Processing

Raw RGB images were processed by the Texas A&M AgriLife Research Corpus Christi Digital Agriculture Laboratory using the methodology described previously [16] and shown in Figure 2. shows the overall pipeline of processing Raw RGB images using Agisoft Metashape software (Agisoft LLC, St. Petersburg, Russia, 191144) to generate geospatial data, such as orthomosaic, Digital Elevation Model (DEM), and 3D point clouds. The geospatial data products were further processed to generate plot level canopy features using QGIS and in-house pipeline.

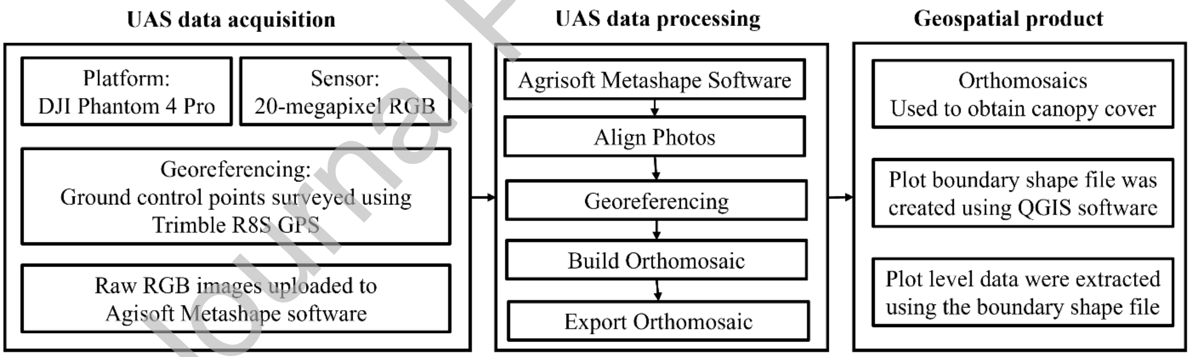

Figure 2. UAS data collection and processing workflow describing the steps from UAS data acquisition to UAS image processing and geospatial data product.

Canopy cover (CC) was derived from the orthomosaic images by applying a Canopeo algorithm to perform a binary image classification, where the RGB orthomosaic imagery was separated into canopy and non-canopy pixels (i.e. plant and soil), then dividing the total number of canopy pixels by the total number of pixels within a plot [27]. This approach was chosen for its robustness in high-resolution imagery, where the distinct color contrast between green plant tissue and the soil background allows for accurate pixel separation. Green leaf area duration (LAD) was visually scored from orthomosaic imagery on a 1-9 scale, where 1 represents early loss of green color and 9 represents late persistence of green CC, based on the timing of canopy color transition, serving as a breeder-oriented phenological proxy for canopy persistence rather than a direct measurement of leaf area index (LAI). Green leaf area duration is used as a visual proxy for canopy greenness duration and does not represent the classical definition of LAD calculated as the integral of leaf area index over time. In this study, senescence is operationally defined as the decline in green CC detected from RGB imagery and reflects loss of chlorophyll rather than physical loss of plant biomass.

2.4 Canopy Cover Modeling and Feature Extraction

Multi-temporal CC data were modeled using a double sigmoid function to capture the distinct phases of canopy development, including growth, plateau, and senescence [13], as shown in equations 1-3. Parameters extracted from the fitted curves included maximum growth rate date (MGRD), MGR, maximum decrease rate date (MDRD), maximum decrease rate (MDR), start linear stage (SLS), start linear stage rate (SLSR), end linear stage (ELS), end linear stage rate (ELSR), start decrease stage (SDS), start decrease stage rate (SDSR), end decrease stage (EDS), end decrease stage rate (EDSR), and DUR. These features were used in subsequent multivariate analyses. Figure 3 shows an example of a fitted double sigmoid curve for a dryland plot of genotype TAM 114 in 2019. The high R^2 (>0.95) and low root mean square error (RMSE) values indicate a good fit, validating the modeling approach.

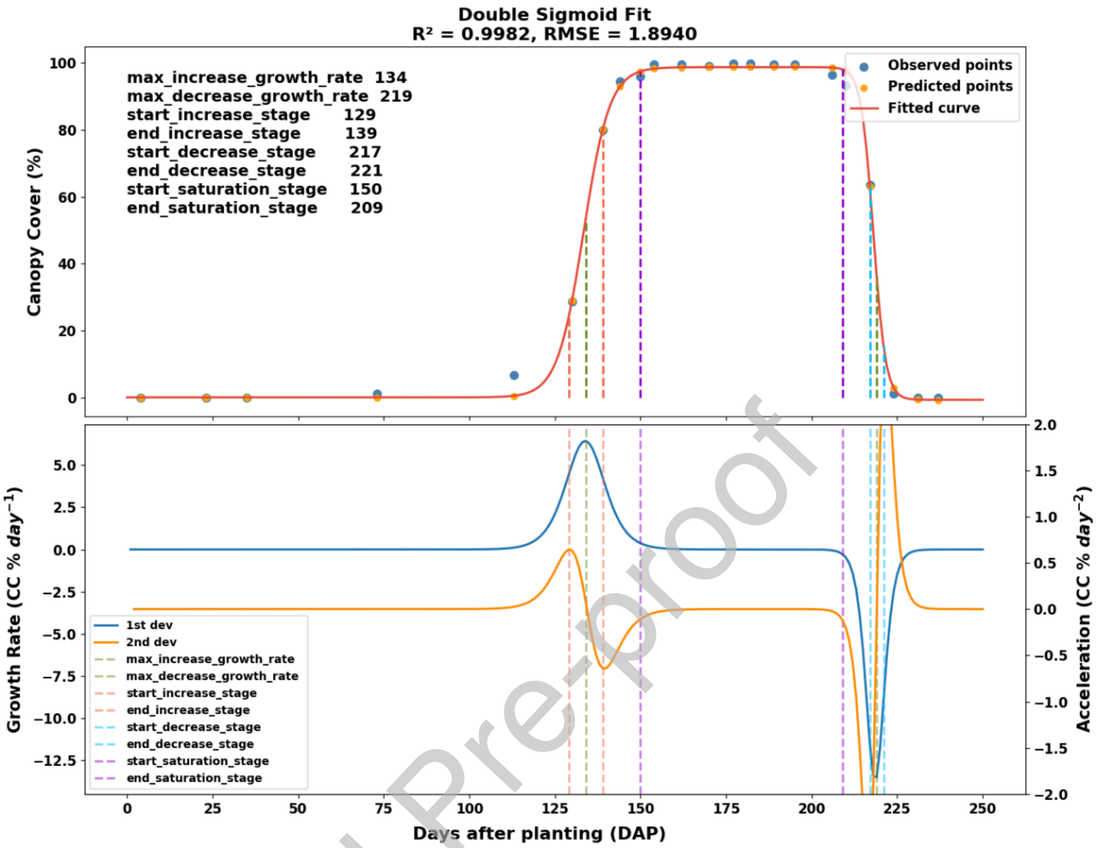

Figure 3. Fitted double sigmoid curve of wheat average canopy cover (%) over the 2019 dryland growing season in Bushland, TX.

$$\boldsymbol{sigmoid_1 = \frac{1}{1+exp(-a_1 \times (x-c_1))}} \tag{1}$$

where: a_1: steepness of the first sigmoid, c_1: center point of the first sigmoid

$$\boldsymbol{sigmoid_2 = \frac{1}{1+exp(-a_2 \times (x-c_2))}} \tag{2}$$

where: a_2: steepness of the second sigmoid, c_2: center point of the second sigmoid

$$\boldsymbol{double\ sigmoid = sigmoid_1 \times (1 - sigmoid_2)} \tag{3}$$

This function delineates two key sigmoidal transitions: the initial increase in CC during vegetative growth (stem elongation) in spring, followed by a plateau phase during canopy saturation, and a subsequent decline as senescence progresses toward the end of the season

(Figure 3). The flexibility of the double sigmoid allows for precise representation of the asymmetry and timing in canopy development and decline, accommodating environmental influences and genotypic variation [13]; [28] Double sigmoid model can estimate parameters such as inflection points, rates of change, and maximum CC that are valuable for phenotyping and assessing plant growth stages under variable conditions [29].

In Figure 3, the first derivative represents the rate of CC change, identifying growth and senescence phases, while the second derivative highlights inflection points that mark key transition stages in the canopy development curve. In the upper panel, blue dots represent observed data points, and orange dots are predicted values used for extracting canopy growth features. In the lower panel, first (blue) and second (orange) derivatives of the double sigmoid fit for average CC (%). Maximum increase growth rate, maximum decrease growth rate, start increase stage, end increase stage, SDS, EDS, start saturation stage, and end saturation stage are marked with dashed lines. The first derivative represents the instantaneous rate of change in CC, with peaks corresponding to periods of rapid growth or senescence. For instance, the maximum value of the first derivative during the ascending phase typically coincides with the period of stem elongation and leaf expansion, while a sharp decline in the descending phase indicates the onset of senescence. The second derivative, representing the acceleration or deceleration of canopy dynamics, is particularly valuable for detecting transition points between growth stages. Inflection points, where the second derivative crosses zero, mark the transition between accelerating and decelerating growth phases. These points often align with critical phenological stages, such as heading, which occurs near the peak of canopy expansion when growth rate begins to slow.

Identification of inflection points in the double sigmoid model is based on the fitted function and its derivatives, rather than on individual observation dates. Consequently, estimation of growth and senescence transition points integrates information across the full time series and is less sensitive to modest variation in observation intervals. Provided that observations adequately span the onset, peak, and decline of CC, which was achieved in this study, the model reliably identifies phenological transitions without requiring uniform temporal spacing.

Each parameter derived from the double sigmoid model corresponds to a distinct and agronomically meaningful phase of winter wheat development. Parameters describing the increasing phase of the curve (e.g., MGR and timing of the linear stage) reflect canopy expansion during stem elongation and early reproductive development, when leaf area accumulation and radiation interception are maximized. Parameters associated with canopy saturation occur near heading, when canopy closure is achieved and further increases in green cover are limited. In contrast, parameters describing the decreasing phase of the curve (e.g., start and end of the decrease stage and MDR) quantify the onset, duration, and intensity of senescence, processes that govern post-anthesis photosynthetic duration and carbohydrate remobilization during grain filling. Collectively, these parameters provide a physiologically interpretable description of canopy development that aligns with established agronomic understanding of winter wheat growth.

2.5 Statistical Analysis

Analysis of variance (ANOVA) was conducted separately for each environment-year using a randomized complete block design with genotypes as fixed and replications as random effects, implemented in SAS 9.4 PROC GLM with significance assessed at $p < 0.05$. A combined analysis across years and water regimes was evaluated but not implemented due to unequal genotype representation among environment-years and strong heterogeneity of variances, particularly in the 2020 dryland trial where extreme drought and freeze stress suppressed genotypic differentiation. These conditions violate key assumptions required for valid combined ANOVA and genotype × environment interaction testing. Therefore, each environment-year was analyzed separately, which is consistent with standard practice in breeding and high-throughput phenotyping studies using contrasting environments.

Pearson Correlation Coefficient was calculated using PROC CORR function in SAS. Repeatability of canopy-derived traits was estimated within each environment using linear mixed-effects models fitted by restricted maximum likelihood in the R package lme4, with genotype specified as a random effect [30]. Repeatability was calculated as the ratio of genotypic variance to total phenotypic variance adjusted for replication and was not estimated for 2020 dryland, where genotypic variance was not detectable.

K-means clustering was performed on the data using R [31]. This combination of unsupervised methods was selected to first identify natural groupings of genotypes with similar performance profiles based on their derived growth traits (k-means) and then to visualize these clusters and interpret which specific traits were the primary drivers of their separation (principal component analysis; PCA biplot). The optimal number of clusters (k=3) was determined using the elbow method, which identified a clear inflection point in the within-cluster sum of squares. The clusters were visualized using a biplot generated by the ggbiplot2 package [32].

3. Results

3.1 Analysis of Variance of Agronomic Traits

Analysis of variance revealed highly significant genotype effects for yield, heading, and LAD across all environments except 2020 dryland (Table 3). Replication effects were generally smaller and only significant in some environments, such as yield in 2019 dryland. Heading date showed the strongest and most consistent genotypic differentiation, with very high F-values ($p < 0.001$), low CVs (<1%), indicating excellent precision. LAD also showed significant genotypic variation in most environments ($p < 0.001$), except for 2020 dry, reflecting stronger environmental influence that season. Together, these results indicate that while genotypic differences were robust for most traits and environments, extreme drought and freeze stress in 2020 dryland reduced the ability to detect genetic variation, particularly for yield and LAD (Table 3). The lack of significant genotypic effects in the 2020 dryland environment further supports the decision to avoid pooled multi-environment analyses, as this environment did not meet the assumptions required for meaningful genotype × environment inference.

Table 3. Mean square of wheat grain yield, heading date (day of year), and green leaf area duration (LAD) of the Texas A&M uniform variety trial in dryland and irrigated environments in 2019 and 2020 at Bushland, TX.

Source	DF	Trait	2019 Dryland	2019 Irrigated	2020 Dryland	2020 Irrigated
Genotype	27	Yield	0.521***			
Genotype	32	Yield		0.595***		
Genotype	33	Yield			0.082	
Genotype	35	Yield				1.874***
Replication	2	Yield	0.361**	0.585**	0.199	2.520***
Residual	54	Yield	0.056			
Residual	64	Yield		0.092		
Residual	66	Yield			0.165	
Residual	70	Yield				0.171
Genotype	27	Heading	9.469***			
Genotype	32	Heading		17.790***		
Genotype	33	Heading			4.442	
Genotype	35	Heading				8.765***
Replication	2	Heading	0.369	1.949	6.657	0.676
Residual	54	Heading	0.381			

Residual	64	Heading		0.731		
Residual	66	Heading			4.990	
Residual	70	Heading				0.619
Genotype	27	LAD	3.571***			
Genotype	32	LAD		2.912***		
Genotype	33	LAD			0.989	
Genotype	35	LAD				3.514***
Replication	2	LAD	1.393	0.253	1.529	3.528*
Residual	54	LAD	1.010			
Residual	64	LAD		0.544		
Residual	66	LAD			0.630	
Residual	70	LAD				1.080

Significance levels: * = $p < 0.05$; * *= $p < 0.01$; *** = $p < 0.001$.

3.2 Ground Reference Measurements

Table 4 summarizes the average grain yield, heading date, and LAD of wheat plots grown under dryland and irrigated conditions in Bushland, TX, during the 2019 and 2020 seasons. Under both environments, yield was higher in 2019 compared to 2020, with the irrigated 2019 trial producing the highest average yield (6.76 T ha^{-1}), while irrigated 2020 had the lowest (2.15 T ha^{-1}). This highlights the limited water stress impact when irrigation was not available during the critical stem elongation and jointing stage due to pandemic staffing restrictions during 2020. Heading dates were later in 2020 across both environments, due to an earlier planting date in the fall of 2019 than the 2019 harvested trial. LAD values were generally higher in 2019 than in 2020, particularly under dryland conditions, reflecting a longer duration of green CC during the more favorable 2019 season. These results highlight the significant influence of year-to-year environmental variation on key agronomic and phenological traits.

Table 4. Average grain yield (T ha^{-1}), heading date (day of year), and green leaf area duration (LAD) of the Texas A&M uniform variety trial in dryland and irrigated environments in 2019 and 2020 at Bushland, TX.

Environment	Year	Yield (T ha^{-1})	Heading Date (DOY)	LAD (1-9)
Dryland	2019	4.73	189	5.25
	2020	2.3	195	4.36
Irrigated	2019	6.76	177	4.29
	2020	2.15	192	5.6

DOY: day of year, LAD: green leaf area duration

3.3 Canopy Cover Distribution

The seasonal CC (%) dynamics of the UVT under dryland and irrigated conditions in 2019 and 2020 at Bushland, TX are shown in Figure 4. The plot shows the progression of average CC (%) over the growing season (Days After Planting) for all genotypes in the uniform variety trials. The dashed line indicates the mean CC at each measurement date, while the blue shaded area represents two standard deviations, illustrating the variation among genotypes. In both years, irrigated plots exhibited faster canopy development, more uniform canopy closure, and sustained high CC levels compared to dryland plots. In 2019, canopy closure occurred earlier and was maintained longer under both environments, especially under irrigation, where CC exceeded 90% for an extended period. In contrast, 2020 showed a delay in canopy development and an earlier onset of senescence, particularly under dryland conditions, where CC declined more abruptly. These patterns highlight that environmental conditions in 2020 were less favorable for maximum CC and grain filling, directly contributing to the reduced yield observed that year. The consistent and extended CC under irrigation, especially in 2019, aligns with the higher yield potential observed in that environment. In all years the observed values mostly fell within two standard deviations of the mean (blue shaded area).

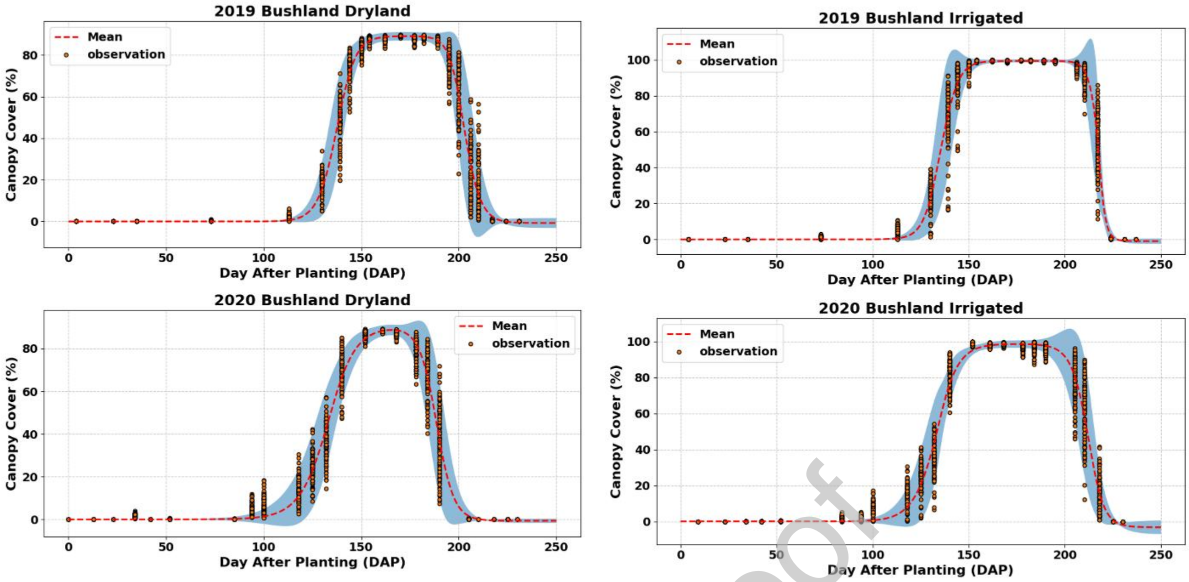

Figure 4. Mean seasonal canopy cover (%) dynamics for dryland and irrigated uniform variety trials across the 2019 and 2020 seasons in Bushland, TX.

3.4 Fitted Canopy Cover Curve

The double-sigmoid function effectively modeled the seasonal growth dynamics of winter wheat CC across all genotypes and environments (Figure 5). The double sigmoid model provided an excellent fit for CC across all environments, with R^2 values exceeding 0.99 in 2019 (0.9981 in dryland and 0.9982 in irrigated) and slightly lower but still strong fits in 2020 (0.9934 in dryland and 0.9908 in irrigated). Root mean square error (RMSE) values ranged from 1.7324 (under 2019 dryland) to 4.0579 (2020 irrigated). The higher RMSE in 2020 irrigated reflects greater variability in CC trajectories among genotypes, likely due to the challenging environmental conditions of that season, including a winter-onset drought and subsequent limitations in spring irrigation. In contrast, the more consistent precipitation events of 2019 allowed the model to capture canopy dynamics with minimal error. Overall, these results indicate that the double sigmoid function reliably described canopy expansion, saturation, and decline dynamics across diverse environments while still reflecting year-to-year variability in crop development. This high degree of accuracy allowed for the reliable characterization of the complete growth cycle, from initial establishment through vegetative growth, canopy saturation, and senescence.

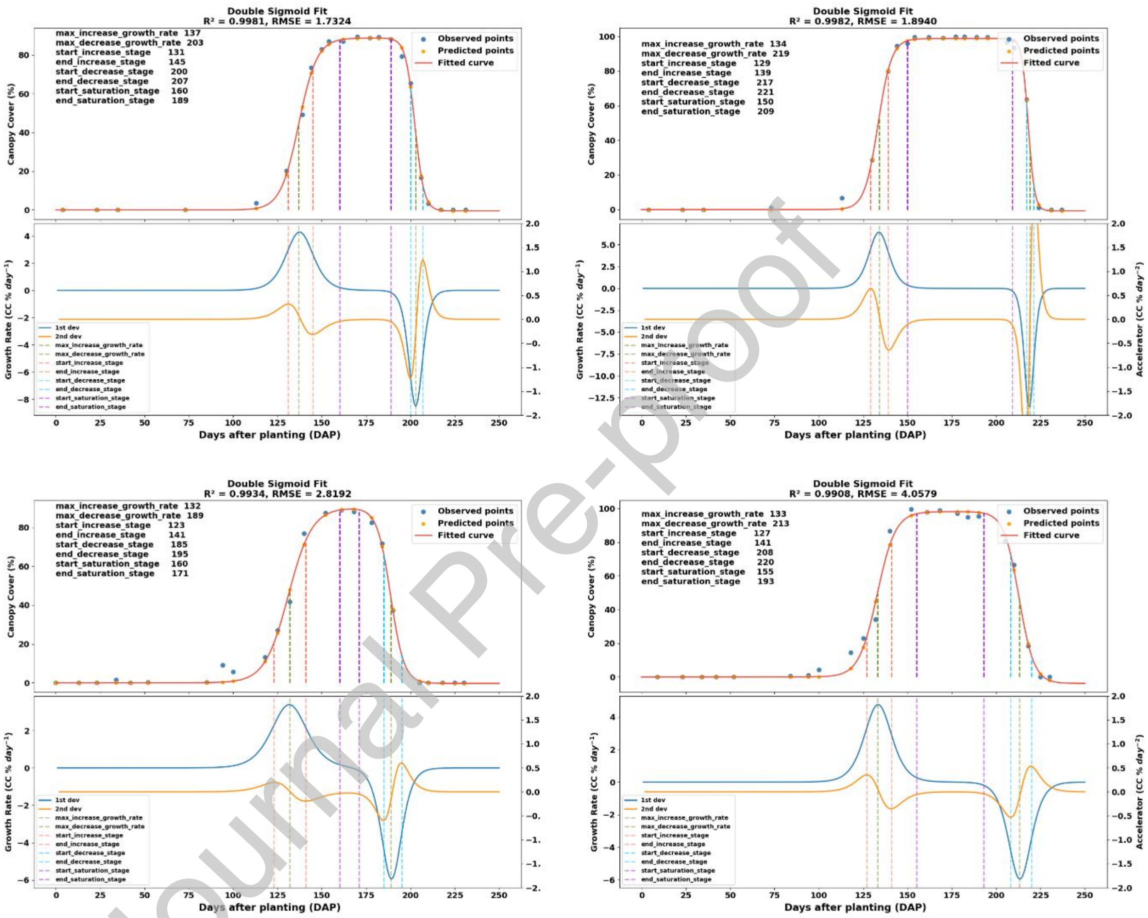

Figure 5. Double-sigmoid model fits for wheat uniform variety trials in 2019 dryland (upper left), 2019 irrigated (upper right), 2020 dryland (lower left) and 2020 irrigated (lower right) conditions in Bushland, TX.

Figure 5 illustrates canopy dynamics across environments, with the extracted canopy traits listed in Table 5. This figure demonstrates the model's application to individual CC (%) time-series data. For each genotype shown, the observed data points (orange circles) are fitted with a double-sigmoid function (solid red line), with the model's predicted points overlaid in blue. The lower panel for each genotype displays the first derivative (growth rate, CC % day^{-1}; orange line) and the second derivative (acceleration of growth, CC % day^{-2}; blue line), which quantify dynamic changes in the growth trajectory. Key growth stages, extracted from the model's derivatives, are indicated by vertical dashed lines: start of increase (green), end of increase (purple), start of decrease (red), end of decrease (blue), start of saturation (orange), and end of saturation (brown). Model performance metrics, including the coefficient of determination (R^2) and root mean square error (RMSE), are displayed in each panel. The most pronounced effect observed was the impact of irrigation on DUR and senescence. In 2019, irrigation significantly extended DUR by 18 days compared to the dryland treatment (73 vs. 55 days). This extension was primarily driven by a 16-day delay in the onset of senescence, or the SDS, which occurred at 214 DAP under irrigation versus 198 DAP in the dryland trial. Interestingly, while senescence was delayed, its maximum rate (MDR) was more than double in the irrigated trial (-32 vs. -15), indicating a much more rapid canopy decline once it began.

Table 5. Values of canopy cover growth curve traits derived from double-sigmoid modeling of UAS imagery of the Texas A&M uniform variety trial in dryland and irrigated environments in 2019 and 2020 at Bushland, TX. Traits represent maximum canopy growth and decline rates, timing and rate of linear and decrease stages, and total canopy duration.

Trait Name	Abbreviation	Units	2019		2020	
			Dryland	Irrigated	Dryland	Irrigated
Maximum growth rate date	MGRD	DAP	137	135	133	133
Maximum growth rate	MGR	% CC day^{-1}	11	15	7.7	11
Maximum decrease rate date	MDRD	DAP	203	216	189	212
Maximum decrease rate	MDR	% CC	-15	-32	-13	-16
Start linear stage	SLS	DAP	131	129	123	125
Start linear stage rate	SLSR	% CC day^{-1}	7.5	10	5.08	7.14
End linear stage	ELS	DAP	143	141	142	140
End linear stage rate	ELSR	% CC day^{-1}	7.61	9.97	5.09	7.06
Start decrease stage	SDS	DAP	198	214	183	206
Start decrease stage rate	SDSR	% CC day^{-1}	-10	-22	-9	-10
End decrease stage	EDS	DAP	208	219	194	217
End decrease stage rate	EDSR	% CC day^{-1}	-10	-22	-9	-10
Duration	DUR	Days	55	73	41	66

Contrasting yearly precipitation also strongly influenced growth dynamics. The 2020 season was demonstrably more stressful, particularly under dryland conditions. Compared to 2019, the 2020 dryland crop exhibited a 15-day earlier onset of senescence (183 vs. 198 DAP) and a 14-day shorter DUR (41 vs. 55 days). The MGR) was also substantially lower in the 2020 dryland, reflecting less vigorous spring growth. These model-derived parameters successfully transform the continuous CC curve into a set of discrete, analyzable traits that quantify the crop's response to its environment and are suitable for subsequent correlation analysis.

To visually illustrate how the double-sigmoid model captures genotypic differences in senescence behavior across environments, fitted canopy cover time-series curves are shown for representative genotypes exhibiting contrasting senescence patterns under both rainfed and irrigated conditions (Figure 6). TAM 204 is an early- to medium-maturing genotype [33], whereas TAM 115 is later maturing, providing a contrasting maturity background for evaluating senescence dynamics. Across both water regimes, the fitted curves clearly resolve differences in the timing and progression of canopy decline between genotypes, demonstrating that the model captures environmentally dependent expression of senescence rather than a single, fixed trajectory. This figure is intended to illustrate model behavior and genotype contrast across environments rather than to represent exhaustive genotype comparisons.

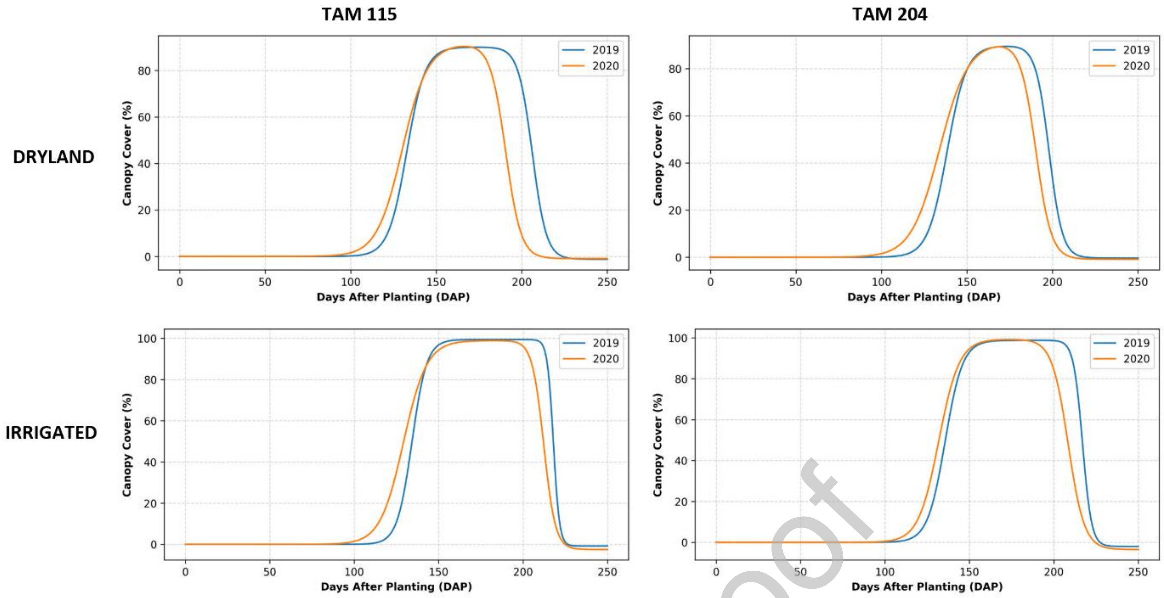

Figure 6. Double-sigmoid model fits for TAM 115 in dryland (upper left), TAM 115 in irrigated (lower left), TAM 204 in dryland (upper right), and TAM 204 in irrigated (lower right), conditions in Bushland, TX in 2019 (blue) and 2020 (orange).

The primary advantage of this modeling approach is the ability to extract key quantitative phenological traits by analyzing the first and second derivatives of the fitted curves. Figure 5 demonstrates how these derivatives pinpoint critical growth stages for each environment-year, including the timing of maximum vegetative growth rate and the onset of canopy senescence. These model-derived parameters serve as quantitative proxies for complex developmental stages, transforming the continuous CC curve into a set of discrete, analyzable traits for subsequent analysis.

The breeding relevance of stay-green traits is inherently context-dependent. Under rainfed conditions, delayed senescence and extended DUR were consistently associated with higher grain yield, reflecting the importance of sustained photosynthetic activity during grain filling under water limitation. Under irrigated conditions, however, the relationship between canopy persistence and yield was more variable, likely reflecting differences in sink strength among genotypes. Prolonged canopy greenness without sufficient sink capacity may not translate into yield gains under optimal resource availability. Accordingly, the stay-green-related traits identified in this study are most appropriately viewed as indicators of stress adaptation and yield stability rather than as universal selection targets across all production environments.

3.5 Pearson Correlation of Canopy Growth Parameters and Reference Measurements with Yield

To evaluate the behavior of single-time-point CC measurements, Pearson's correlation coefficients between CC and grain yield were calculated for each acquisition date across environments (Figure 7). Correlation strength varied substantially over time, with significant positive associations observed only during narrow temporal windows that differed by year and water regime. In 2019 dryland, the strongest correlations occurred during mid-to-late reproductive stages, whereas irrigated environments showed weaker and less consistent relationships across dates. In the 2020 dryland environment, correlations between single-date CC and yield were generally low and unstable across the season, due to drought and unavailability of irrigation at spring green-up.

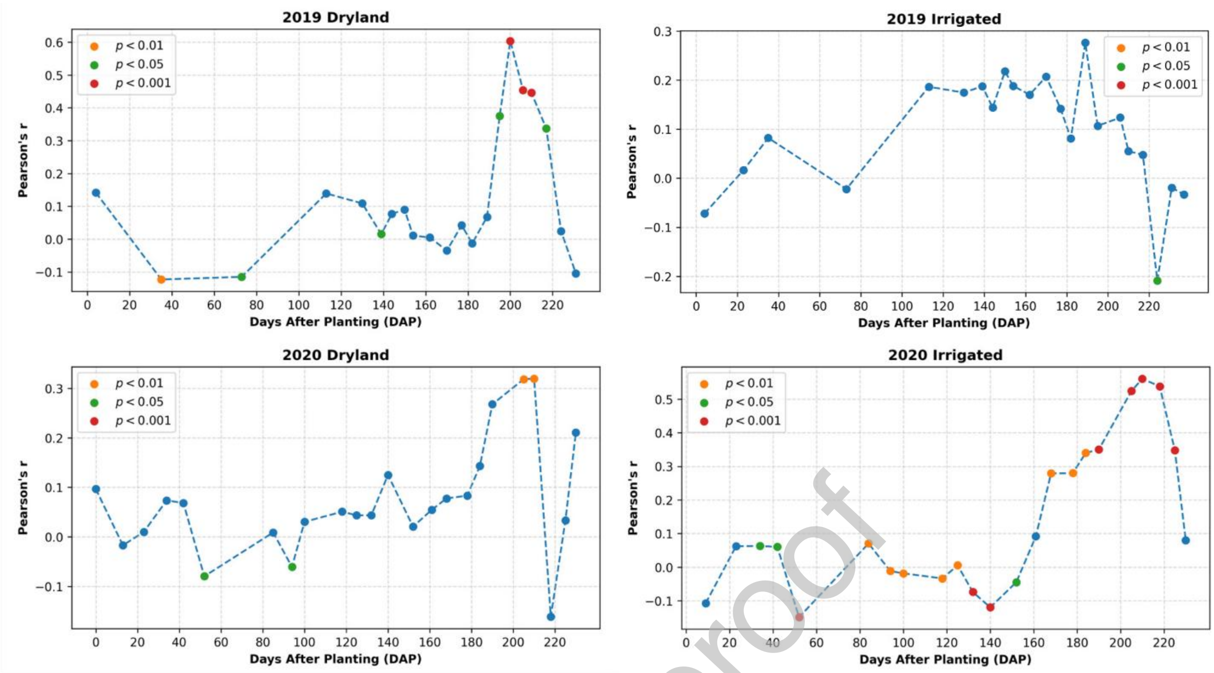

Figure 7. Pearson correlation matrix of yield, heading and green leaf area duration (LAD) with canopy growth features extracted from a double sigmoid function for 2019 and 2020 Bushland, TX dryland wheat plots.

These results demonstrate that correlations derived from single-date CC measurements are highly dependent on acquisition timing and environmental conditions, with no single date consistently providing strong associations with yield across environments. Outside of these limited windows, correlations were weak or non-significant, indicating that single-time-point CC captures only transient canopy states rather than integrated seasonal processes related to yield formation. In contrast to these temporally constrained relationships, time-series-derived canopy traits integrate information across the growing season, enabling consistent characterization of canopy dynamics across environments.

Figure 8 presents the Pearson correlation matrices between yield, heading date, and LAD and canopy growth features derived from a double sigmoid model for dryland wheat plots in 2019 and 2020. In 2019, several canopy features showed strong positive correlations with yield. Of note, the end of the decrease stage (r=0.56), start of the decrease stage (r=0.46), and duration of CC (r=0.36) were all positively associated with yield, indicating that delayed senescence and longer DUR contributed to higher productivity. Similarly, the MDRD (r=0.55) and MDR (r=0.35) also correlated positively with yield, suggesting that the timing and pattern of canopy decline were important determinants of grain filling success. In contrast, in 2020, the correlations between yield and canopy traits were generally weaker and more variable. The end of decrease stage remained moderately correlated with yield (r=0.32), but other features showed only weak or non-significant associations. This breakdown in trait-yield relationships in 2020 reflects water limitation stress and variability, diminishing the predictive value of canopy traits under dryland conditions.

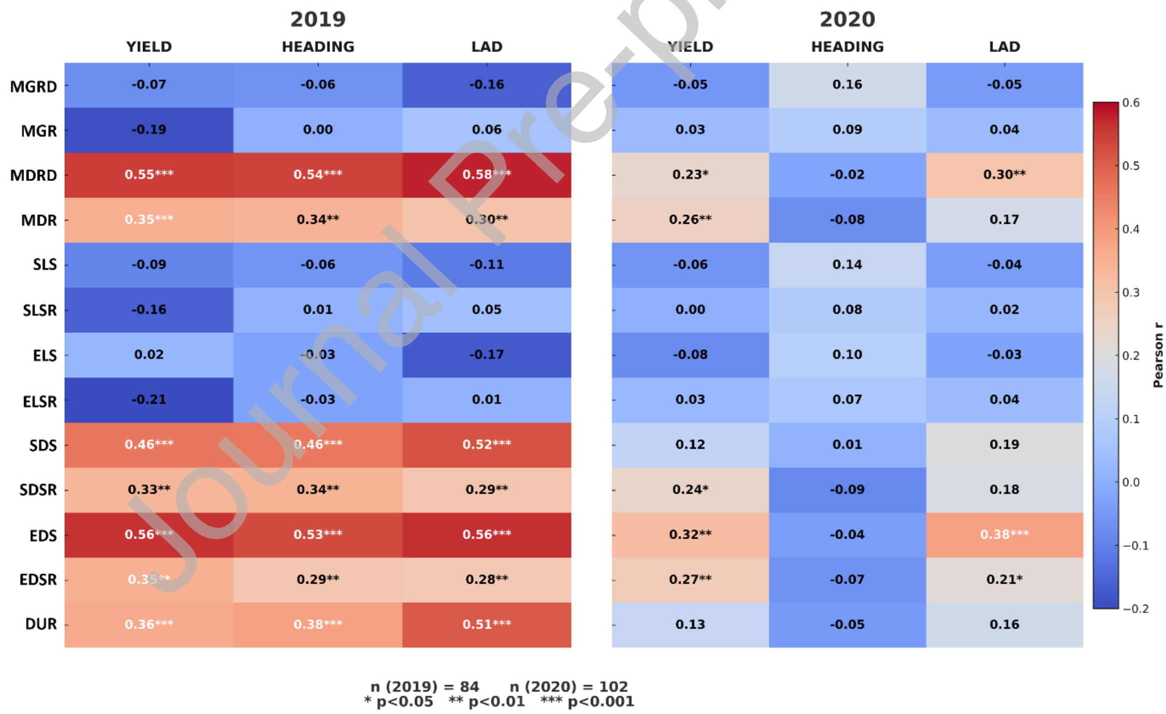

Figure 8. Pearson correlation matrix of yield, heading and green leaf area duration (LAD) with canopy growth features extracted from a double sigmoid function for 2019 and 2020 Bushland, TX dryland wheat plots.

The contrast between water regimes was most pronounced in 2019. Under rainfed conditions, yield showed strong positive correlations with late-season canopy traits, including SDS, EDS, and DUR (Figure 8). In contrast, correlations between yield and senescence-related traits were weaker or negative under irrigated conditions in the same year (Figure 9), indicating that canopy persistence traits were most informative for yield differentiation under rainfed stress in 2019.

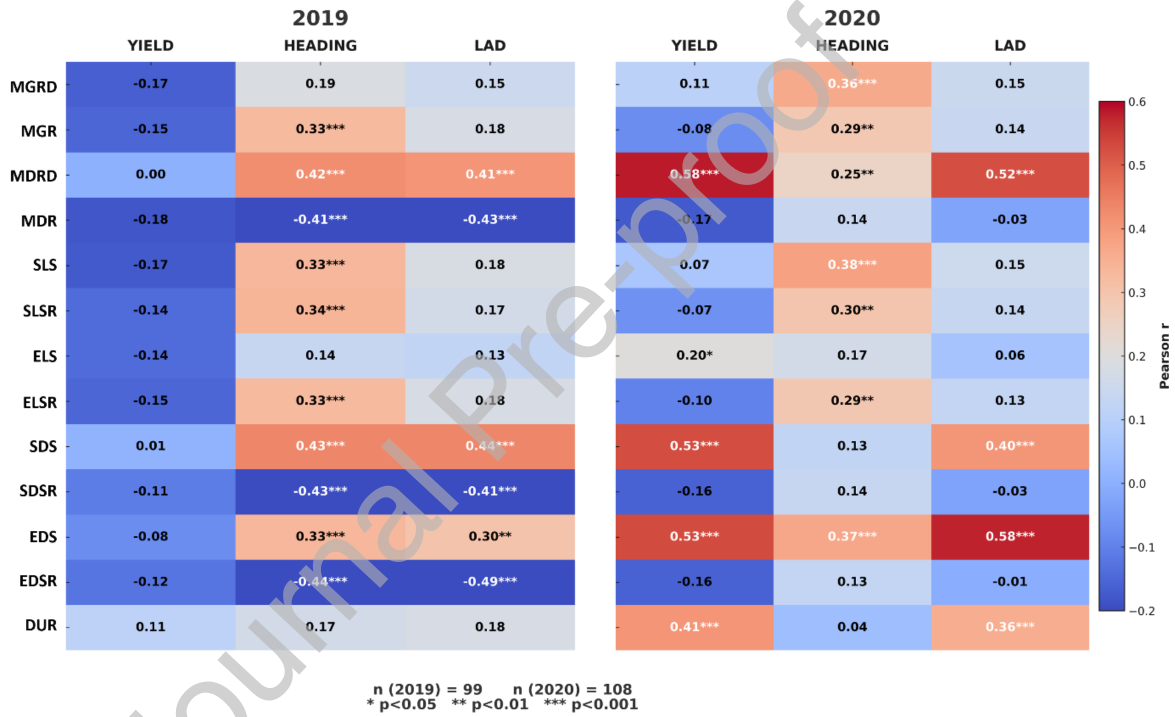

Figure 9. Pearson correlation matrix of yield, heading, and green leaf area duration (LAD) with canopy growth features extracted from a double sigmoid function for 2019 and 2020 Bushland, TX irrigated wheat plots.

Irrigated trial Pearson correlation metrices between yield, heading date, green leaf area duration (LAD), and canopy growth features for irrigated wheat plots in 2019 and 2020 are shown in Figure 9. In 2019, yield exhibited negative correlations with several early and late canopy dynamics, particularly the MDR (r=-0.18) and end of the decrease stage rate (r=-0.12), suggesting that rapid canopy senescence and abrupt declines in cover were detrimental to yield under irrigated conditions. In contrast, positive yield correlations were observed with duration (r=0.11), implying that extended canopy saturation modestly benefited grain production. In 2020, yield associations with canopy features were much stronger. The start of the decrease stage showed the strongest positive correlation with yield (r=0.53), followed by SDSR (r=0.40), EDS (r=0.32), and duration (r=0.41). These results highlight the importance of sustained canopy function during the post-anthesis period for yield formation under irrigation, especially in a drought-stress year like 2020, where sink demand was likely not fully saturated. The greater consistency and strength of correlations in 2020 reflects more pronounced variation among genotypes in response to environmental constraints, allowing canopy traits to more clearly differentiate yield outcomes.

3.6 Repeatability of UAS-Derived Canopy Traits

Repeatability of UAS-derived canopy traits was moderate to high across environments where genotypic variance was detectable (Table 6). Timing-based traits, including DUR, SDS, and EDS, exhibited consistently high repeatability (R = 0.82-0.96), while rate-based traits showed slightly greater environmental sensitivity but remained highly repeatable in most environments. In contrast, repeatability could not be reliably estimated for the 2020 dryland environment because genotypic variance approached zero for most canopy traits, consistent with the lack of significant genotype effects observed for agronomic traits in that environment.

Table 6. Repeatability of canopy cover growth curve traits derived from double-sigmoid modeling of UAS imagery of the Texas A&M uniform variety trial in dryland and irrigated environments in 2019 and 2020 at Bushland, TX. Traits represent maximum canopy growth and decline rates, timing and rate of linear and decrease stages, and total canopy duration.

Trait Name	Abbreviation	2019	2020

		Dryland	Irrigated	Dryland	Irrigated
Maximum growth rate date	MGRD	0.90	0.88	NA*	0.95
Maximum growth rate	MGR	0.91	0.86	NA	0.96
Maximum decrease rate date	MDRD	0.94	0.93	NA	0.69
Maximum decrease rate	MDR	0.92	0.94	NA	0.66
Start linear stage	SLS	0.87	0.84	NA	0.79
Start linear stage rate	SLSR	0.85	0.82	NA	0.77
End linear stage	ELS	0.89	0.86	NA	0.81
End linear stage rate	ELSR	0.86	0.83	NA	0.78
Start decrease stage	SDS	0.88	0.93	NA	0.81
Start decrease stage rate	SDSR	0.84	0.81	NA	0.74
End decrease stage	EDS	0.96	0.85	NA	0.65
End decrease stage rate	EDSR	0.83	0.80	NA	0.72
Duration	DUR	0.89	0.89	NA	0.82

* Genotypic variance not detectible

3.7 Genotype Clustering and Trait Association.

To further explore the relationships among canopy dynamics, yield, and phenological traits, principal component analysis (PCA) with k-means clustering (k=3) was conducted for each environment-year combination (Figure 10). Across both years and water regimes, yield consistently co-clustered with the canopy-duration and late-senescence timing traits; duration, SDS, and EDS in the PC1-PC2 space. This tight, repeatable grouping suggests that genotypes maintaining a green canopy for longer and delaying the onset and termination of decline tend to produce higher grain yields. The heading and linear-stage traits SLS, ELS, SLSR, and ELSR formed a separate cluster. The rate traits that measure how quickly the canopy grows or senesces (growth and decline rates; maximum growth rate date, MGR, MDRD, and MDR, SDSR and EDSR) fell between the phenology traits and the duration/late-senescence traits in the PCA, indicating they describe the speed of change rather than directly tracking final yield.

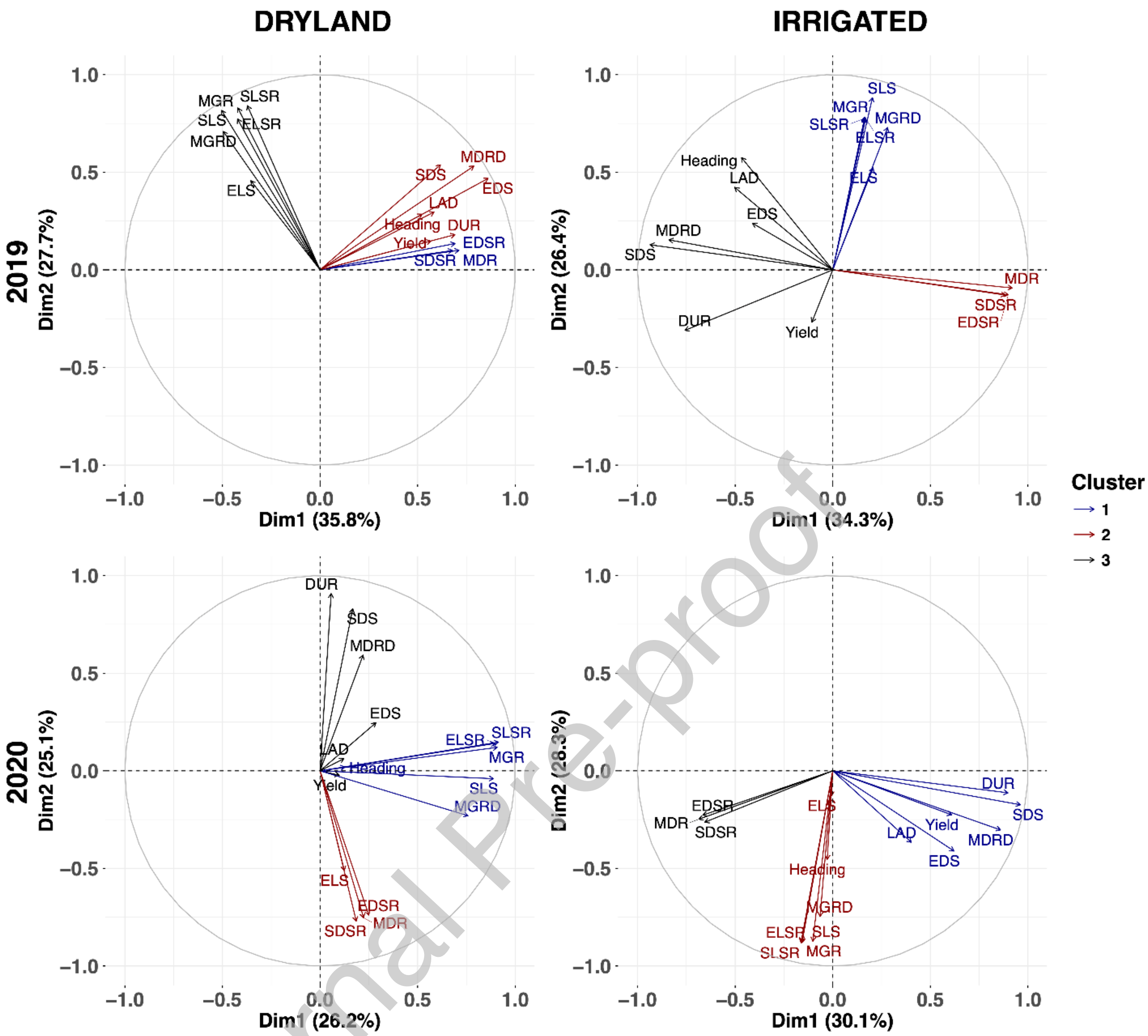

Figure 10. Principal component analysis with k-means clusters of yield, heading, and green leaf area duration (LAD) with canopy growth features extracted from a double sigmoid function for 2019 and 2020 Bushland, TX dryland and irrigated wheat plots. MGRD = maximum growth rate date; MGR = maximum growth rate; MDRD = maximum decrease rate date; MDR = maximum decrease rate; SLS/ELS = start/end of linear stage; SLSR/ELSR = rate at start/end of linear stage; SDS/EDS = start/end of decrease stage; SDSR/EDSR = rate at start/end of decrease stage; DUR = duration.

Heading clustered uniformly with the linear-stage timing traits and rates (SLS, SLSR, ELS, and ELSR) and remained clearly separated from the yield-duration cluster in every environment-year (Figure 10). This pattern shows that heading is primarily associated with the timing of rapid canopy expansion rather than the persistence of green leaf area, reinforcing its role as a phenological trait largely independent of yield.

Green leaf area duration was related to the yield-duration cluster, SDS, and EDS across all year-environments (Figure 10). The repeated co-location of LAD with duration/late-decline traits indicates that canopy persistence can serve as proxy for yield potential in these trials, whereas linear-stage phenology traits remained on a distinct axis and rate traits again showed bridging behavior.

To identify genotypes with distinct growth strategies, k-means clustering was performed on the 13 UAS-derived traits. The analysis successfully partitioned the germplasm into groups that represent clear performance archetypes, with the top-ranking genotypes for each trait and environment summarized in Table 7. A consistent genetic signal for late senescence emerged from the k-cluster analysis. Winterhawk repeatedly clustered with late-season traits, ranking as a top performer for EDS in 2019 and 2020 dryland, and 2020 irrigated. This indicates a stable stay-green characteristic that persists across different seasonal conditions. Other genotypes, such as PlainsGold Canvas and Smith's Gold, also consistently appeared in this late-senescing group.

Table 7. Top-Ranking Genotypes from K-Means Clustering for All UAS-Derived Traits. This table lists the top unique genotypes that clustered most closely with each of the 13 phenological and growth rate traits across dryland and irrigated conditions in 2019 and 2020 wheat growing seasons in Bushland, TX.

Trait	2019 Dryland	2019 Irrigated	2020 Dryland	2020 Irrigated
Early-Season Growth & Vigor				
SLS	LCS Pistol Bentle Iba	DH12HRW27-3 LCS Pistol Iba	CP7010 TAM 114 OK12206-2	SY Monument Winterhawk SY Wolverine
SLSR	LCS Pistol Bentley Iba	DH12HRW27-3 Iba LCS Pistol	SY Wolverine CP7010 T158	SY Grit CP7010 SY Wolverine

ELS	LCS Pistol Bentley PlainsGold Canvas	DH12HRW27-3 LCS Pistol Iba	CP7010 TAM 114 OK12206-2	SY Monument, Winterhawk, SY Wolverine
ELSR	LCS Pistol Bentley PlainsGold Canvas	LCS Pistol Iba DH12HRW27-3	SY Wolverine CP7010 T158	SY Grit CP7010 SY Wolverine
MGRD	LCS Pistol Bentley PlainsGold Canvas	LCS Pistol DH12HRW27-3 Iba	OK12206-2 SY Grit LCS Mint	CP7010 PlainsGold Canvas TAM 112
MGR	LCS Pistol Bentley PlainsGold Canvas	LCS Pistol Iba DH12HRW27-3	SY Wolverine CP7010 T158	SY Grit CP7010 SY Wolverine
Late-Season Senescence & Persistence				
SDS	Smith's Gold CP7869 Winterhawk	WB 4792 Dyna-Gro Long Branch PlainsGold Avery	OK168512 Baker's Ann CP7050AX	OK16729W WB 4303 SY Monument
SDSR	Smith's Gold Winterhawk LCS Chrome	WB 4792 Dyna-Gro Long Branch PlainsGold Avery	Baker's Ann CP7050AX OK168512	Lonerider Spirit Rider Showdown
EDS	Winterhawk Smith's Gold TAM 115	PlainsGold Canvas CPX79-10 TAM 205	Winterhawk CP7017AX PlainsGold Canvas	OK12206-2 WB 4792 Winterhawk
EDSR	TAM 115 CPX79-10 WB 4792	TAM 304 CP7909 TAM 112	TAM 114 CP7010 WB 4792	Lonerider Showdown TX14V70214
MDRD	Winterhawk Smith's Gold CP7869	WB 4792 Dyna-Gro Long Branch PlainsGold Avery	Baker's Ann SY Monument OK168512	PlainsGold Canvas SY Monument Iba
MDR	CPX79-10 WB 4792 TAM 115	TAM 112 CP7909 TAM 113	CP7010 TAM 114 OK12206-2	Lonerider Showdown Spirit Rider
Overall Canopy Duration				
DUR	TAM 115 CPX79-10 WB 4792	TAMW-101 TAM 111 LCS Link	CP7050AX LCS Mint OK168512	WB 4303 OK16729W Showdown

MGRD = maximum growth rate date; MGR = maximum growth rate; MDRD = maximum decrease rate date; MDR = maximum decrease rate; SLS/ELS = start/end of linear stage; SLSR/ELSR = rate at start/end of linear stage; SDS/EDS = start/end of decrease stage; SDSR/EDSR = rate at start/end of decrease stage; DUR = duration.

In contrast, early-season growth strategies showed strong genotype-by-environment (G×E) interaction. In the 2019 trials, LCS Pistol frequently clustered with early vigor traits such as MGR and an early ELS in both irrigated and dryland conditions. However, under the drought-stressed environmental pressures of 2020, a completely different set of genotypes, primarily SY Wolverine and CP7010, emerged as the architypes for this rapid establishment profile.

This environmental dependency was most pronounced for overall DUR, where the top-ranking genotypes were almost entirely different across each of the four environment-years (Table 7). This demonstrates that the optimal strategy for maintaining a long-lasting canopy is highly specific to the seasonal conditions. This clustering approach effectively deconstructs the complex performance data, allowing for the identification of specific genotypes that exemplify desirable growth architectures, such as stable late senescence or environment-specific early vigor, for targeted breeding selection.

4. Discussion

The advent of high-throughput phenotyping (HTP) platforms, particularly those utilizing UAS, has revolutionized the capacity of plant breeders to assess crop performance at scale [5–7,14,16,18,18]. However, the sheer volume of temporal data generated necessitates the use of advanced analytical methods to distill meaningful biological insights. In this study, we demonstrated the successful application of a double-sigmoid function to model the temporal dynamics of CC in a large panel of winter wheat genotypes under varying water availability. This approach not only provides an exceptionally accurate fit to the observed data ($R^2 > 0.99$) but also enables the extraction of key phenological parameters directly relevant to breeding for yield and climate resilience. Canopy cover metrics are especially valuable for assessing phenology in water-limited environments, where stress can accelerate development and premature senescence.

4.1 Agronomic Traits and Environmental Context

The agronomic data emphasize the environmental contrasts between 2019 and 2020, which shaped yield and phenological expression. Yields were consistently higher in 2019 across both dryland and irrigated conditions, with irrigated 2019 producing the most (6.76 T ha^{-1}). In contrast, 2020 yields were reduced by limited rainfall and irrigation challenges during jointing and stem elongation, despite a significant increase in irrigation water over 2019. The later heading date observed in 2020 relative to 2019 is an artifact of an earlier planting date in the fall, rather than a true environmental effect, because heading is expressed in days after planting (DAP). The 2020 season began with adequate soil moisture for stand establishment, but limited precipitation during the winter accelerated crop development due to water stress. The 2020 dryland genotypes were further stressed by a late-season freeze on April 13. Due to advanced phenological development, wheat heads were damaged in earlier-maturing genotypes, resulting in lower yields, earlier canopy decline, and lower LAD values in 2020. These differences establish the context for interpreting canopy dynamics, developmental timing, and their relationships to yield. The lack of significant genotypic effects for yield, heading, and LAD in the 2020 dryland environment supports this interpretation, indicating that the severe drought and freeze stress masked underlying genetic differences.

Rather than treating year and water regime as factors in a pooled statistical model, this study intentionally uses these environments as contrasting stress scenarios to evaluate the stability and environmental sensitivity of canopy-derived traits. Consistent associations between late-season canopy persistence traits and yield across multiple environment-years indicate biologically meaningful genotype responses, even when formal genotype × environment interaction terms cannot be validly estimated.

Although canopy cover and derivative parameters were not destructively validated against leaf area index (LAI) in this study, their biological relevance is supported by their consistent alignment with independently measured agronomic traits and expected physiological patterns. CC extraction was conducted using the Canopeo algorithm, which has been independently validated in wheat and other crops under comparable imaging conditions. In addition, the binary classified images (green vs. non-green pixels) were manually inspected to verify accurate segmentation and ensure that vegetation and background pixels were correctly classified under field conditions. The double-sigmoid parameters showed consistent and biologically meaningful alignment with manually recorded heading dates, particularly near the inflection point corresponding to the onset of canopy decline. Furthermore, canopy duration and late-senescence timing traits exhibited strong and repeatable correlations with grain yield across favorable and stress-prone environments.

From a breeding perspective, the objective of these traits is not to replace physiological measurements such as LAI, but to provide scalable, repeatable proxies of canopy persistence and senescence timing suitable for large multi-genotype trials. Future work incorporating destructive LAI sampling or handheld canopy measurements would further refine biological calibration; however, the consistent genotype differentiation and agronomic associations observed here support their utility for selection decisions.

4.2 The Double-Sigmoid Model: A Superior Tool for Capturing the Full Crop Life Cycle

The biological relevance of the double sigmoid parameters can be interpreted in the context of distinct winter wheat growth stages, linking canopy expansion to stem elongation, canopy saturation to heading, and canopy decline to senescence and grain filling. A primary goal with this work is to use a double-sigmoid model to characterize the entire seasonal trajectory of canopy development. Much of the previous research on modeling crop growth has relied on single-sigmoid functions (such as logistic or Gompertz models), which are effective at describing the vegetative growth phase but fail to adequately capture the crucial senescence phase post-anthesis [13,14]. This limitation is significant, as the timing and rate of senescence are critical determinants of the grain-filling duration and, consequently, final yield. Our model overcomes this by integrating both the growth and senescence phases into a single, cohesive function. This holistic view enables the precise quantification of the start, end, and duration of the canopy's life, providing a more comprehensive picture of the genotype's strategy for resource capture and allocation. By extracting traits such as DUR, a parameter derived directly from the model, this approach allows breeders to select for specific physiological mechanisms. In moving beyond single-point measurements, this high-throughput phenotyping approach provides quantitative parameters that are powerful predictors of key agronomic outcomes in winter wheat. The model not only accurately described the growth dynamics but also revealed how the timing and rate of specific growth phases are intrinsically linked to yield, phenology, and the plant's response to environmental stress. The low RMSE values (1.73-4.06) across different environments and genotypes further validate the model's robustness and its suitability for genetic studies where G × E interactions exist.

Before interpreting individual correlation coefficients, it is important to clarify the conceptual advantage of the time-series approach relative to single-date CC measurements. Although several individual canopy-derived parameters showed moderate correlation coefficients, this is expected for traits that describe distinct components of canopy development rather than a single integrative outcome. Single-time-point CC measurements capture only a transient canopy state and are highly sensitive to acquisition timing, phenological differences among genotypes, and short-term environmental conditions. In contrast, time-series modeling integrates canopy dynamics across the full season, enabling separation of growth timing, growth rate, and senescence behavior. Notably, traits describing late-season canopy persistence and senescence timing exhibited the strongest and most consistent associations with yield, relationships that cannot be captured reliably using a single-date CC measurement. Thus, the value of the time-series approach lies in its biological interpretability and robustness, rather than maximizing correlation from any single canopy observation.

The proximity of heading to the start of the decrease stage inflection points in the curve indicates the potential of using second derivative features from fitted canopy models to infer heading date, especially under water-limited conditions where phenological transitions are more closely coupled with physiological decline (Figure 5). Bhandari et al. [16] found that drought-stressed wheat reached heading earlier and senesced faster than irrigated wheat, with CC declining about a week sooner and reaching near-zero green cover roughly 7 days earlier. UAS-derived canopy curves captured these shifts quantitatively, showing that slower canopy decline after heading correlated with higher grain yield ($r^2 = 0.65$), highlighting the potential of canopy time-series to identify stress-tolerant, stay-green genotypes for breeding. Thus, CC time-series not only mark phenological events, such as heading date and onset of senescence, but also provide integrative measures of stress tolerance that breeders can use to select drought- and heat-tolerant genotypes. Kaushal et al. [5] found that the highest predictive power for wheat yield occurred at the late grain-filling stage (Feekes 11) in South Dakota, underscoring the importance of traits like canopy senescence and grain fill duration. Reed et al. [34] demonstrated that fractional green CC measured at critical growth stages could predict final wheat grain yield in Oklahoma with reasonable accuracy.

4.3 Relationship between Extracted Features and Agronomic Traits

Comparing dryland and irrigated environments across 2019 and 2020 shows differences in how canopy development features relate to yield. In 2019, the dryland trial showed the strongest and most consistent positive correlations between yield and canopy traits, particularly those associated with late-season canopy persistence, such as the end of decrease stage, maximum decrease date, and duration, suggesting that genotypes maintaining green cover longer under limited water conditions had higher yield potential. In contrast, irrigated 2019 plots showed generally weaker or negative correlations with yield, indicating that the favorable environment may have reduced the selective pressure on DUR. However, in 2020, this pattern shifted. Under irrigated conditions, yield correlations with canopy features became stronger and more aligned with those observed in dryland 2019. Traits such as the start of decrease stage, duration, and SDSR were positively associated with yield, highlighting the importance of prolonged canopy function under stress, even with irrigation. Meanwhile, the dryland 2020 trial showed the weakest overall correlations, likely due to greater environmental stress or measurement noise obscuring the trait-yield relationships. Overall, these results suggest that the predictive value of canopy traits is water-stress-dependent, with late-season canopy dynamics being particularly valuable indicators of yield potential under water-limited or stressful conditions. While early-season vigor sets the threshold, a slow decrease rate allows time for carbohydrates to translocate from the stem to the grain [35]. A steep rate of CC decrease is influenced more by water or heat stress than by plant maturity.

From a crop breeding perspective, the primary value of the double sigmoid framework lies in its ability to transform high-frequency UAS imagery into physiologically interpretable, quantitative traits that can be used for selection prior to harvest. Traits describing DUR and senescence timing provide objective proxies for grain-filling potential and stress tolerance, particularly under water-limited environments where late-season canopy persistence is closely associated with yield stability. These traits can be used to rank genotypes within a season, identify parents with complementary growth and senescence strategies, and reduce reliance on destructive or low-throughput phenotyping methods. Importantly, the time-series nature of the model allows breeders to distinguish genotypes with similar end-point yields but contrasting developmental trajectories, supporting more informed advancement decisions.

The weakening of correlations between canopy-derived traits and grain yield in 2020 can be explained by well-established physiological responses of wheat to combined drought, heat, and freeze stress during reproductive development. Water limitation and elevated temperatures accelerate phenological development and promote premature senescence, reducing the effective grain-filling period even in genotypes that maintain green CC. In addition, freeze damage during heading and early anthesis can directly impair spike fertility and kernel set, creating yield losses that are independent of post-anthesis canopy persistence. Under these conditions, DUR and senescence timing no longer serve as reliable proxies for assimilate supply to the grain, as sink capacity becomes the dominant yield-limiting factor. Similar decoupling of stay-green traits from yield under severe stress has been reported in wheat and other cereals, where canopy greenness may persist despite irreversible reproductive damage or limited carbohydrate translocation.

4.4 Implications of Canopy-Derived Traits for Wheat Breeding

The high repeatability observed for canopy-derived timing traits confirms that the double-sigmoid framework captures stable, genetically structured variation in canopy development across environments (Table 6). Traits related to canopy persistence and senescence timing (DUR, SDS, and EDS) were particularly robust, supporting their suitability for selection within breeding nurseries. The inability to estimate repeatability in the 2020 dryland environment reflects extreme environmental stress rather than limitations of the phenotyping approach. Severe drought combined with a late freeze compressed phenological variation and masked genetic differences, a pattern also evident in the agronomic trait analyses. Similar reductions in genetic signals under extreme stress have been widely reported in multi-environment breeding trials and highlight the importance of evaluating canopy traits across diverse but informative environments.

Repeatability analysis demonstrated that UAS-derived canopy traits captured stable, genetically structured variation within environments, particularly for DUR and senescence timing traits (SDS and EDS). The high repeatability of these traits indicates that genotype rankings are reliable, enabling breeders to use canopy persistence as a practical selection criterion to identify superior lines prior to harvest and to increase selection intensity while reducing reliance on resource-intensive yield measurements. In contrast, growth and senescence rate traits showed lower repeatability and greater environmental sensitivity, limiting their utility for direct selection but retaining value for characterizing growth strategies. The absence of detectable repeatability in the 2020 dryland environment reflects extreme stress masking genetic differences rather than limitations of the phenotyping approach.

4.5 Principal Component Analysis and K-means Cluster: From Model Parameters to Identifiable Agronomic Traits

Figure 10 shows a consistent structure across both years and water regimes. Yield aligns closely with canopy-duration and late-senescence timing traits, including DUR, SDS, and EDS. In contrast, heading clusters with early linear-stage timing traits such as SLS, ELS, SLSR, and ELSR. The growth-rate traits occupy intermediate positions, describing how quickly the canopy develops or declines rather than the persistence traits that most directly track yield. Practically, this indicates that a compact index composed of duration, SDS, and EDS could serve as a high-throughput proxy for yield potential. Heading showed weaker predictive power but consistently clustered with early canopy expansion traits, reinforcing its role as a developmental timing trait rather than a yield determinant.

Environmental contrasts help explain subtle shifts. 2019 was cooler, with adequate season-long precipitation (Figure 1) and high grain yields (Table 4); the 2019 irrigated trial was free of water stress. Under those favorable conditions, the yield-duration cluster is compact and clearly separated from the phenology axis. In 2020, the crop faced winter-long water stress, minimal precipitation at anthesis and grain filling, and a late-season freeze during heading (April 13, 2020). Drought accelerated maturity, disproportionately impacting early-maturing genotypes, and the freeze precipitated an even earlier canopy decline than drought alone. These pressures positioned some decline-related traits closer to the yield-duration group and compressed senescence timing. However, the core association of yield with DUR and late decline remained intact. The consistency of that relationship across favorable and stress-prone seasons underscores the utility of UAS-derived canopy-curve traits to improve selection accuracy: they are objective, scalable, and capture time-series physiology that traditional single-date approaches miss.

The primary success of this methodology lies in its ability to generate reliable proxies for grain yield. Our results show strong and consistent positive correlations between senescence-related traits and grain yield under rainfed and stress-prone environments, whereas relationships under irrigated conditions were more variable (Figures 6 and 7). This provides a quantitative, high-throughput method for characterizing the "stay-green" phenomenon, particularly in environments where stress during grain filling limits photosynthetic duration. For a breeder, this means that instead of waiting for harvest, they can use UAS imagery to identify genotypes with a longer grain-filling period, a key driver of yield potential.

Beyond serving as a yield proxy, the approach provides the resolution needed to categorize genotypes into meaningful performance archetypes. The k-means clustering analysis (Table 7) grouped genotypes based on their entire growth profile, identifying distinct strategies. Genotypes like Winterhawk consistently exhibited a late-senescence profile across multiple environments, making them ideal for breeding programs targeting drought tolerance. In contrast, other genotypes, like LCS Pistol in 2019 and SY Wolverine in 2020, showed early vigor by means of a high MGR. Furthermore, the analysis provided key insights into lines from the Texas A&M breeding program. For instance, TAM 114 and TAM 205 demonstrated strong early-season vigor traits in the more stressful 2020 dryland environment, identifying them as valuable genetic resources for rapid establishment under challenging conditions. This demonstrates the model's utility in identifying specific physiological architecture for targeted selection.

The model was sensitive enough to capture the significant impact of year-to-year weather variations on crop phenology. The 2020 growing season was marked by a winter-onset drought, followed by an inability to fully irrigate during spring green-up. The effect of these stressors is clearly quantified by the model's outputs. In the 2020 dryland trial, the winter drought led to a 15-day earlier onset of senescence (SDS at 183 DAP) and a 14-day shorter DUR compared to 2019. Furthermore, the limited spring irrigation in 2020 explains why the irrigated trial DUR (66 days) failed to match the persistence of the 2019 irrigated trial (73 days). This ability to quantify the impact of specific environmental events on growth dynamics is invaluable, as it allows breeders to assess genotype performance under realistic, stress-inducing field conditions.

4.6 Limitations and Data Considerations

Results are based on two years at a single location (Bushland, TX) under contrasting water regimes; additional environment-years are required to assess the stability and generality of model-derived traits across broader genetic backgrounds and management systems. The unsupervised clustering used here identifies associations among traits rather than direct predictive accuracy for future seasons. True prediction will require supervised models trained and validated across years, with explicit management of collinearity among time-series-derived variables. Parameter estimation is also sensitive to temporal data density and curve-fitting assumptions, and irregular data acquisition remains a persistent challenge in multi-temporal UAS phenotyping. Extreme stress events, such as the combined drought and freeze observed in 2020, can shift canopy trajectories and partially decouple canopy persistence traits from grain yield. While excluding such seasons may improve model clarity, these conditions reflect production realities and cannot always be avoided.

4.7 Breeding Implications and Future Research

From a breeding perspective, the primary value of this framework lies in its ability to differentiate genotypes based on growth and senescence strategies rather than single end-point traits (e.g., grain yield). Time-series-derived canopy parameters enable classification of genotypes into physiologically meaningful groups (e.g., early-vigorous, late-senescing, short-duration types), providing actionable information for parent selection and advancement decisions under variable water availability. By linking canopy dynamics to yield and phenological traits, this framework provides breeders with actionable information for parent selection and advancement decisions, particularly under variable water availability. Importantly, the approach is scalable and resource-efficient: meaningful canopy dynamics can be captured using low-cost RGB imagery with weekly or biweekly flights targeted to key developmental stages, and the modeling framework can be applied retrospectively to existing image datasets. Future research should extend this analysis across multiple locations and seasons to quantify genotype-by-environment interactions, evaluate trait repeatability, and define minimum temporal sampling requirements. Integration of double-sigmoid-derived canopy traits with genomic prediction and environmental covariates represents a promising direction for improving selection accuracy in operational breeding pipelines.

5.0 Conclusion

This study demonstrates that the double-sigmoid function is a robust and reliable model for characterizing the complete seasonal winter wheat crop growth dynamics of winter wheat using UAS-derived CC data. The model effectively captures key phases, including vegetative growth, canopy saturation, and senescence, enabling the extraction of valuable quantitative phenological traits. The strong fit of the model across diverse environments ($R^2 > 0.99$) validates its application in high-throughput phenotyping pipelines.

Model-derived traits, particularly those related to DUR and the timing of senescence, showed strong and significant correlations with grain yield, especially under favorable conditions such as 2019 dryland and 2020 irrigated. In contrast, the limited water stress and freeze stress during 2020 suppressed genotypic differentiation, resulting in weak or non-significant trait-yield relationships. This divergence highlights the model's ability to differentiate environmental effects and a genotype's response to stress.

The ability of the double sigmoid model to provide a continuous, high-resolution description of the crop lifecycle represents a significant advance over traditional single-sigmoid models. By providing quantitative metrics for traits such as the onset of senescence and the rate of senescence, this approach offers breeders an objective, high-throughput tool for identifying genotypes with desirable grain-filling periods and stress resilience, particularly under water-limited environments.

Future research should integrate these model-derived traits with genomic data and multi-environment weather information to identify loci governing canopy dynamics and environmental responsiveness. Expanding analyses across more locations and years will further enhance the utility of this framework for breeding climate-resilient winter wheat cultivars.

Funding

This research was partially funded by Texas Governor's University Research Initiative (GURI), Texas Wheat producer's board. This project was supported by the Agriculture and Food Research Initiative Competitive Grant 2022-68013-36439 (WheatCAP) from the USDA National Institute of Food and Agriculture.

CRediT authorship contribution statement

S Baker Writing – Original draft, Methodology, Investigation, Formal analysis, Data curation
L Zhao, Methodology, Writing – review & editing, Software
J Landivar Scott, Writing – review & editing, software
J Rudd, Writing – Review & editing, Supervision, Funding acquisition, Formal analysis, Conceptualization
A MH Ibrahim, Writing – Review & editing, Funding acquisition
J Landivar, Writing – Review & editing, Funding acquisition
J Jung, Writing – review & editing,
S Liu, Writing – review & editing
K Nowka, Writing – review & editing
M Bhandari, Writing – review & editing, Supervision, Funding acquisition, Formal analysis, Conceptualization

Declaration of Competing Interest

The authors declare that they have no known competing financial interests or personal relationships that could have appeared to influence the work reported in this paper.

Acknowledgements

The authors would like to acknowledge all the wheat breeding staff and student workers at Texas A&M AgriLife Research Amarillo, particularly Mr. Jason Baker, student workers and staff at Texas A&M AgriLife Research Corpus Christi, particularly Dr. Anjin Chang.

Statement on AI Use

AI was used to assist with coding, formatting, and grammatical editing.

References

[1] United States Department of Agriculture, National Agricultural Statistics Service (USDA NASS). Data & Statistics 2025.
[2] United States Department of Agriculture NASS. Texas Wheat Varieties: 2024 Wheat Variety Survey. Austin, TX: USDA NASS, Southern Plains Regional Field Office; 2024.
[3] Ayankojo IT, Thorp KR, Thompson AL. Advances in the Application of Small Unoccupied Aircraft Systems (sUAS) for High-Throughput Plant Phenotyping. Remote Sens 2023;15:2623. https://doi.org/10.3390/rs15102623.
[4] Hassan MA, Yang M, Rasheed A, Jin X, Xia X, Xiao Y, et al. Time-Series Multispectral Indices from Unmanned Aerial Vehicle Imagery Reveal Senescence Rate in Bread Wheat. Remote Sens 2018;10. https://doi.org/10.3390/rs10060809.
[5] Kaushal S, Gill HS, Billah MM, Khan SN, Halder J, Bernardo A, et al. Enhancing the potential of phenomic and genomic prediction in winter wheat breeding using high-throughput phenotyping and deep learning. Front Plant Sci 2024;15.
[6] Shi Y, Thomasson JA, Murray SC, Pugh NA, Rooney WL, Shafian S, et al. Unmanned Aerial Vehicles for High-Throughput Phenotyping and Agronomic Research. PLOS ONE 2016;11:e0159781. https://doi.org/10.1371/journal.pone.0159781.
[7] Bhandari M, Chang A, Jung J, Ibrahim AMH, Rudd JC, Baker S, et al. Unmanned aerial system-based high-throughput phenotyping for plant breeding. Plant Phenome J 2023;6:e20058. https://doi.org/10.1002/ppj2.20058.
[8] Christopher JT, Christopher MJ, Borrell AK, Fletcher S, Chenu K. Stay-green traits to improve wheat adaptation in well-watered and water-limited environments. J Exp Bot 2016;67:5159–72. https://doi.org/10.1093/jxb/erw276.
[9] Pinto RS, Reynolds MP, Mathews KL, McIntyre CL, Olivares-Villegas J-J, Chapman SC. Heat and drought adaptive QTL in a wheat population designed to minimize confounding agronomic effects. Theor Appl Genet 2010;121:1001–21. https://doi.org/10.1007/s00122-010-1351-4.
[10] Thapa S, Xue Q, Jessup KE, Rudd JC, Liu S, Marek TH, et al. Yield determination in winter wheat under different water regimes. Field Crops Res 2019;233:80–7. https://doi.org/10.1016/j.fcr.2018.12.018.
[11] Damgaard C, Weiner J. Modeling the growth of individuals in crowded plant populations. J Plant Ecol 2008;1:111–6. https://doi.org/10.1093/jpe/rtn008.
[12] Taiz L, Zeiger E, Møller IM, Murphy A. Plant Physiology and Development. 6th ed. Sunderland, MA: Sinauer Associates; 2015.
[13] Soltani A, Sinclair TR. Modeling Physiology of Crop Development, Growth and Yield. CAB International; 2012.
[14] Bhandari M, Ibrahim AMH, Xue Q, Jung J, Chang A, Rudd JC, et al. Assessing winter wheat foliage disease severity using aerial imagery acquired from small Unmanned Aerial Vehicle (UAV). Comput Electron Agric 2020;176:105665. https://doi.org/10.1016/j.compag.2020.105665.
[15] Rahaman MdM, Chen D, Gillani Z, Klukas C, Chen M. Advanced phenotyping and phenotype data analysis for the study of plant growth and development. Front Plant Sci 2015;6.
[16] Bhandari M, Baker S, Rudd JC, Ibrahim AMH, Chang A, Xue Q, et al. Assessing the Effect of Drought on Winter Wheat Growth Using Unmanned Aerial System (UAS)-Based Phenotyping. Remote Sens 2021;13. https://doi.org/10.3390/rs13061144.

[17] Herr AW, Campbell KG, Li X, Carter AH. Spatial analysis with unoccupied aircraft systems data in wheat breeding yield trials. Plant Phenome J 2024;7:e70007. https://doi.org/10.1002/ppj2.70007.
[18] Herr AW, Schmuker P, Carter AH. Large-scale breeding applications of unoccupied aircraft systems enabled genomic prediction. Plant Phenome J 2024;7:e20101. https://doi.org/10.1002/ppj2.20101.
[19] Roth L, Kronenberg L, Aasen H, Walter A, Hartung J, van Eeuwijk F, et al. High-throughput field phenotyping reveals that selection in breeding has affected the phenology and temperature response of wheat in the stem elongation phase. J Exp Bot 2024;75:2084–99. https://doi.org/10.1093/jxb/erad481.
[20] Zhao L, Guo W, Wang J, Wang H, Duan Y, Wang C, et al. An Efficient Method for Estimating Wheat Heading Dates Using UAV Images. Remote Sens 2021;13. https://doi.org/10.3390/rs13163067.
[21] Ren J, Chen Z, Qingbo Z, Tang H. Regional yield estimation for winter wheat with MODIS-NDVI data in Shandong, China. Int J Appl Earth Obs Geoinformation 2008;10:403–13. https://doi.org/10.1016/j.jag.2007.11.003.
[22] Haghighattalab A, González Pérez L, Mondal S, Singh D, Schinstock D, Rutkoski J, et al. Application of unmanned aerial systems for high throughput phenotyping of large wheat breeding nurseries. Plant Methods 2016;12:35. https://doi.org/10.1186/s13007-016-0134-6.
[23] Myers E, Kerekes J, Daughtry C, Russ A. Assessing the Impact of Satellite Revisit Rate on Estimation of Corn Phenological Transition Timing through Shape Model Fitting. Remote Sens 2019;11. https://doi.org/10.3390/rs11212558.
[24] Evett SR, Marek GW, Copeland KS, Colaizzi PD. Quality Management for Research Weather Data: USDA-ARS, Bushland, TX. Agrosystems Geosci Environ 2018;1:180036. https://doi.org/10.2134/age2018.09.0036.
[25] Evett SR, Copeland KS, Ruthardt BB, Marek GW, Colaizzi PD, Howell TA Sr, et al. Standard quality controlled research weather data - USDA-ARS, Bushland, Texas 2022. https://doi.org/10.15482/USDA.ADC/1526433.
[26] Large EC. GROWTH STAGES IN CEREALS ILLUSTRATION OF THE FEEKES SCALE. Plant Pathol 1954;3:128–9. https://doi.org/10.1111/j.1365-3059.1954.tb00716.x.
[27] Patrignani A, Ochsner TE. Canopeo: A Powerful New Tool for Measuring Fractional Green Canopy Cover. Agron J 2015;107:2312–20. https://doi.org/10.2134/agronj15.0150.
[28] Darvishzadeh R, Matkan AA, Dashti Ahangar A. Inversion of a radiative transfer model for estimation of canopy cover and LAI in wheat. ISPRS J Photogramm Remote Sens 2019;149:1–15.
[29] Verrelst J, Camps-Valls G, Muñoz-Marí J, Rivera JP, Veroustraete F, Clevers JGPW, et al. Optical remote sensing and the retrieval of terrestrial vegetation bio-geophysical properties – A review. ISPRS J Photogramm Remote Sens 2015;108:273–90.
[30] Bates D, Maechler M, Bolker B, Walker S. Fitting Linear Mixed-Effects Models Using lme4. J Stat Softw 2015;67:1–48. https://doi.org/10.18637/jss.v067.i01.
[31] R Core Team. R: A Language and Environment for Statistical Computing. Vienna, Austria: R Foundation for Statistical Computing; 2024.
[32] Wickham H. ggplot2: Elegant Graphics for Data Analysis. Springer-Verlag New York; 2016.

[33] Rudd JC, Devkota RN, Ibrahim AM, Baker JA, Baker S, Sutton R, et al. 'TAM 204' Wheat, Adapted to Grazing, Grain, and Graze-out Production Systems in the Southern High Plains. J Plant Regist 2019;13:377–82. https://doi.org/10.3198/jpr2018.12.0080crc.
[34] Reed V, Arnall B, Finch B, Souza J. Predicting Winter Wheat Grain Yield Using Fractional Green Canopy Cover (FGCC). Int J Agron 2021;2021:1–8. https://doi.org/10.1155/2021/1443191.
[35] Wang Z, Zhang YP, Zhang YH, Xue Q. Remobilization of water soluble carbohydrates in non-leaf organs and contribution to grain yield in winter wheat under reduced irrigation. Int J Plant Prod 2013;7:97–116.

Ethical Statement

The authors declare that all the ethical guidelines provided by the journal are followed with respect to originality of the research, authorship contribution, and the analysis. All authors agreed to the current version of the manuscript. Generative AI was used to support code, grammatical errors.

Declaration of interests

The authors declare that they have no known competing financial interests or personal relationships that could have appeared to influence the work reported in this paper.